

# **Geophysical Research Letters**\*

#### RESEARCH LETTER

10.1029/2023GL106808

#### **Key Points:**

- Aerosol Robotic Networks
   (AERONET) dust retrievals are
   assessed by the thermal infrared (TIR)
   radiative closure study compared with
   the collocated AIRS observations
- The warm bias in the TIR radiative closure suggests the possibility of AERONET underestimating the supercoarse dust
- Adding super-coarse dust to the AER-ONET size distribution improves the TIR closure without deteriorating its inherent retrieval accuracy

#### **Supporting Information:**

Supporting Information may be found in the online version of this article.

#### Correspondence to:

Z. Zhang, zzbatmos@umbc.edu

#### Citation:

Zheng, J., Zhang, Z., DeSouza-Machado, S., Ryder, C. L., Garnier, A., Di Biagio, C., et al. (2024). Assessment of dust size retrievals based on AERONET: A case study of radiative closure from visible-near-infrared to thermal infrared. *Geophysical Research Letters*, 51, e2023GL106808. https://doi.org/10.1029/2023GL106808

Received 24 OCT 2023 Accepted 5 FEB 2024

#### **Author Contributions:**

**Conceptualization:** Jianyu Zheng, Zhibo Zhang

Data curation: Claudia Di Biagio, Ellsworth J. Welton, Hongbin Yu, Africa Barreto, Margarita Y. Gonzalez Formal analysis: Jianyu Zheng, Zhibo Zhang

Funding acquisition: Zhibo Zhang, Hongbin Yu

Investigation: Jianyu Zheng, Zhibo Zhang, Claire L. Ryder, Anne Garnier, Ping Yang, Ellsworth J. Welton

© 2024. The Authors.

This is an open access article under the terms of the Creative Commons

Attribution License, which permits use, distribution and reproduction in any medium, provided the original work is properly cited.

# Assessment of Dust Size Retrievals Based on AERONET: A Case Study of Radiative Closure From Visible-Near-Infrared to Thermal Infrared

Jianyu Zheng<sup>1,2</sup> , Zhibo Zhang<sup>1,3</sup> , Sergio DeSouza-Machado<sup>1,3</sup>, Claire L. Ryder<sup>4</sup> , Anne Garnier<sup>5</sup> , Claudia Di Biagio<sup>6</sup> , Ping Yang<sup>7</sup> , Ellsworth J. Welton<sup>2</sup> , Hongbin Yu<sup>2</sup>, Africa Barreto<sup>8</sup>, and Margarita Y. Gonzalez<sup>9</sup>

<sup>1</sup>Goddard Earth Sciences Technology and Research II, University of Maryland Baltimore County, Baltimore, MD, USA, <sup>2</sup>NASA Goddard Space Flight Center, Greenbelt, MD, USA, <sup>3</sup>Department of Physics, University of Maryland Baltimore County, Baltimore, MD, USA, <sup>4</sup>Department of Meteorology, University of Reading, Reading, UK, <sup>5</sup>Analytical Mechanics Associates, Hampton, VA, USA, <sup>6</sup>Université Paris Cité, University Paris Est Creteil, CNRS, LISA, Paris, France, <sup>7</sup>Department of Atmospheric Sciences, Texas A&M University, College Station, TX, USA, <sup>8</sup>Izaña Atmospheric Research Center (IARC), State Meteorological Agency (AEMET), Santa Cruz de Tenerife, Spain, <sup>9</sup>Atmospheric Research and Instrumentation Branch, National Institute for Aerospace Technology (INTA), Madrid, Spain

**Abstract** Super-coarse dust particles (diameters >10 µm) are evidenced to be more abundant in the atmosphere than model estimates and contribute significantly to the dust climate impacts. Since super-coarse dust accounts for less dust extinction in the visible-to-near-infrared (VIS-NIR) than in the thermal infrared (TIR) spectral regime, they are suspected to be underestimated by remote sensing instruments operates only in VIS-NIR, including Aerosol Robotic Networks (AERONET), a widely used data set for dust model validation. In this study, we perform a radiative closure assessment using the AERONET-retrieved size distribution in comparison with the collocated Atmospheric Infrared Sounder (AIRS) TIR observations with comprehensive uncertainty analysis. The consistently warm bias in the comparisons suggests a potential underestimation of super-coarse dust in the AERONET retrievals due to the limited VIS-NIR sensitivity. An extra super-coarse mode included in the AERONET-retrieved size distribution helps improve the TIR closure without deteriorating the retrieval accuracy in the VIS-NIR.

**Plain Language Summary** Dust particles suspended in the atmosphere span a wide size range (0.001–100 μm). Notably, super-coarse dust particles (diameter >10 μm) have been observed to be more abundant than what climate models suggest. Theoretically, these super-coarse particles present little radiative signatures in visible to near-infrared (VIS-NIR) but significantly affect the thermal infrared (TIR) radiation. This study addresses the question of whether remote sensing techniques operating in the VIS-NIR can capture these dust particles. We use side-by-side observations associated with a dust plume in both VIS-NIR and TIR to assess whether the dust properties, including the size distribution, inferred by VIS-NIR observations can generate well-matched radiative signatures with TIR observations. We found that the simulated outgoing radiation at the top of the atmosphere in TIR using the VIS-NIR-inferred dust properties is greater than the observations because of not enough dust extinction, potentially led by the absence of super-coarse dust. By introducing an extra super-coarse mode in the size distribution, we found a better match with the TIR observation, while the dust optical properties retrieved in VIS-NIR can be mostly conserved. Our result demonstrates the importance of combining VIS-NIR and TIR observations to retrieve the dust size distribution.

#### 1. Introduction

As the most abundant type of atmospheric aerosol in terms of dry mass, mineral dust (referred to as "dust" hereafter) emitted from arid and semi-arid regions is transported by atmospheric winds from local to intercontinental scales, exerting far-reaching impacts on the Earth system (Choobari et al., 2014; Ginoux et al., 2012; Goudie, 1983; Kinne et al., 2006; Tegen & Fung, 1994). Dust particles vary widely in size (particle diameter  $(D_p)$  from 0.001 to 100  $\mu$ m), typically showing a bimodal volume particle size distribution (PSD) with a fine  $(D_p < 1 \ \mu$ m) and a dominant coarse  $(D_p > 1 \ \mu$ m) mode (Mahowald et al., 2014). In situ measurements from recent field campaigns observed prevailing super-coarse dust particles  $(D_p > 10 \ \mu$ m) across the Saharan-to-Atlantic region (Ryder et al., 2013, 2018; van der Does et al., 2016; Weinzierl et al., 2011, 2017), which are

ZHENG ET AL. 1 of 12

Methodology: Jianyu Zheng,
Zhibo Zhang, Sergio DeSouza-Machado.
Claire L. Ryder, Anne Garnier
Software: Jianyu Zheng, Ping Yang
Supervision: Zhibo Zhang
Validation: Jianyu Zheng,
Sergio DeSouza-Machado
Visualization: Jianyu Zheng
Writing – original draft: Jianyu Zheng
Writing – review & editing:
Jianyu Zheng, Zhibo Zhang, Claire
L. Ryder, Anne Garnier, Claudia Di
Biagio, Ping Yang, Ellsworth J. Welton,
Hongbin Yu

often absent in climate model simulations (Adebiyi et al., 2023; Kok et al., 2017). On one hand, this contrast suggests that the mechanisms for emitting and transporting these super-coarse dust particles are missed in model simulations. On the other hand, the limited sampling volume raises concerns about the representativeness of in situ measurements. In this regard, globally distributed ground-based remote sensing measurements, such as Aerosol Robotic Networks (AERONET (Dubovik et al., 2000; Holben et al., 1998)), can retrieve continuous long-term dust properties to achieve reliable statistics. However, AERONET operates in VIS-NIR spectra, where super-coarse dust particles account only for a small fraction of the total extinction within the broad size range (Ryder et al., 2019). Previous studies also suggested limited sensitivities of AERONET AOD measurements in VIS-NIR to coarse mode aerosol properties (Torres & Fuertes, 2021; Torres et al., 2017). This leads to an important question: Are the VIS-NIR-based remote sensing measurements sensitive enough to capture the supercoarse dust in their retrievals?

Numerous studies have compared in situ measurements with AERONET observations, but interpreting these results is challenging due to inherent differences in sampling and uncertainty sources between the two types of measurements (McConnell et al., 2008; Müller et al., 2012; Ryder et al., 2015; Toledano et al., 2019). For example, in situ measurements sample full-size-range dust PSD at a specific range of altitudes within a relatively small volume, with multiple sources of uncertainty from various instruments targeting different size ranges (Reid et al., 2003). Differently, AERONET retrieves column-integrated PSD based on dust's spectral radiative signature at multiple VIS-NIR channels, with uncertainties tied to the observed sky radiances and aerosol optical depth (AOD) measurements, alongside the simultaneously retrieved complex refractive index (CRI) and non-spherical (spheroid) assumptions (Dubovik et al., 2006).

Recent studies suggest that combining VIS-NIR and thermal infrared (TIR) observations provides a unique way to evaluate the full range of dust PSD as TIR observations are chiefly sensitive to coarse and super-coarse modes of dust compared to VIS-NIR observations (Pierangelo et al., 2005; Zheng et al., 2023). For example, Zheng et al. (2022) combined satellite observations from VIS lidar and TIR spectrometer to synergistically retrieve VIS and TIR dust optical depth (DOD). They found that the TIR DOD extrapolated by VIS DOD using the climatological AERONET PSD over Cape Verde (a dust-dominated site) is systematically lower than the satellite-retrieved TIR DOD, implying a lack of coarse particles in the applied PSD. Song et al. (2018) showed that using the in situ measured dust PSD, coarser than that of AERONET, yielded a better agreement with observation-based dust longwave direct radiative effect.

Driven by these studies, we present here a radiative closure case study on whether using the AERONET retrieved dust PSD based on VIS-NIR observation can simulate the TIR brightness temperature (BT) in the 8–13  $\mu m$  window region that matches the observations from the collocated Atmospheric Infrared Sounder (AIRS). We hypothesize that the limited sensitivity to super-coarse particles in AERONET VIS-NIR observations may result in the absence of super-coarse mode dust in the AERONET-retrieved PSD, potentially causing a warm bias in simulated BT compared to AIRS observations. The rest of the paper is organized as follows: the data, radiative transfer models and scattering calculation are introduced in Section 2. The radiative closure implementation and results are presented in Section 3. Discussion and conclusions are drawn in Section 4.

### 2. Data and Model

#### 2.1. AERONET and AIRS Observations

AERONET provides column-integrated AOD measurements through sun photometers (Holben et al., 1998), which is often considered "ground truth" for validations of satellite AOD products (Schuster et al., 2012; Zhou et al., 2020). Additionally, it retrieves aerosol microphysical properties, including PSD and CRI at four VIS-NIR channels (i.e., 440, 675, 870, and 1,020 nm), distributed as Inversion products (Dubovik et al., 2000, 2006). The latest released Version 3 (V3) Level 2 (L2) data, which is used in this study, includes improved cloud screening, quality assurance and reduced uncertainties within minimal uncertainty levels (Giles et al., 2019; Sinyuk et al., 2020). In this study, we use AERONET retrievals for a dust case observed at the Santa Cruz Tenerife (SCT) site (28.473°N, 16.247°W) on 19 June 2022 (see Figure 1a).

Because the current AERONET has no TIR observations, we instead perform the radiative closure via the comparison with the TIR BT at the top of the atmosphere (TOA) observed by AIRS onboard NASA's Aqua satellite. In this study, we use the L1C AIRS data that has the measured global hyperspectral infrared radiances

ZHENG ET AL. 2 of 12

1944/8007, 2024, 4, Downloaded from https://agupubs.onlinelibrary.wiley.com/doi/10.1029/2023GL106808, Wiley Online Library on [18/02/2024]. See the Terms and Conditions (https://onlinelibrary.wiley.com/terms-and-conditions) on Wiley Online Library for rules of use; OA articles are governed by the applicable Creative Commons Licenses

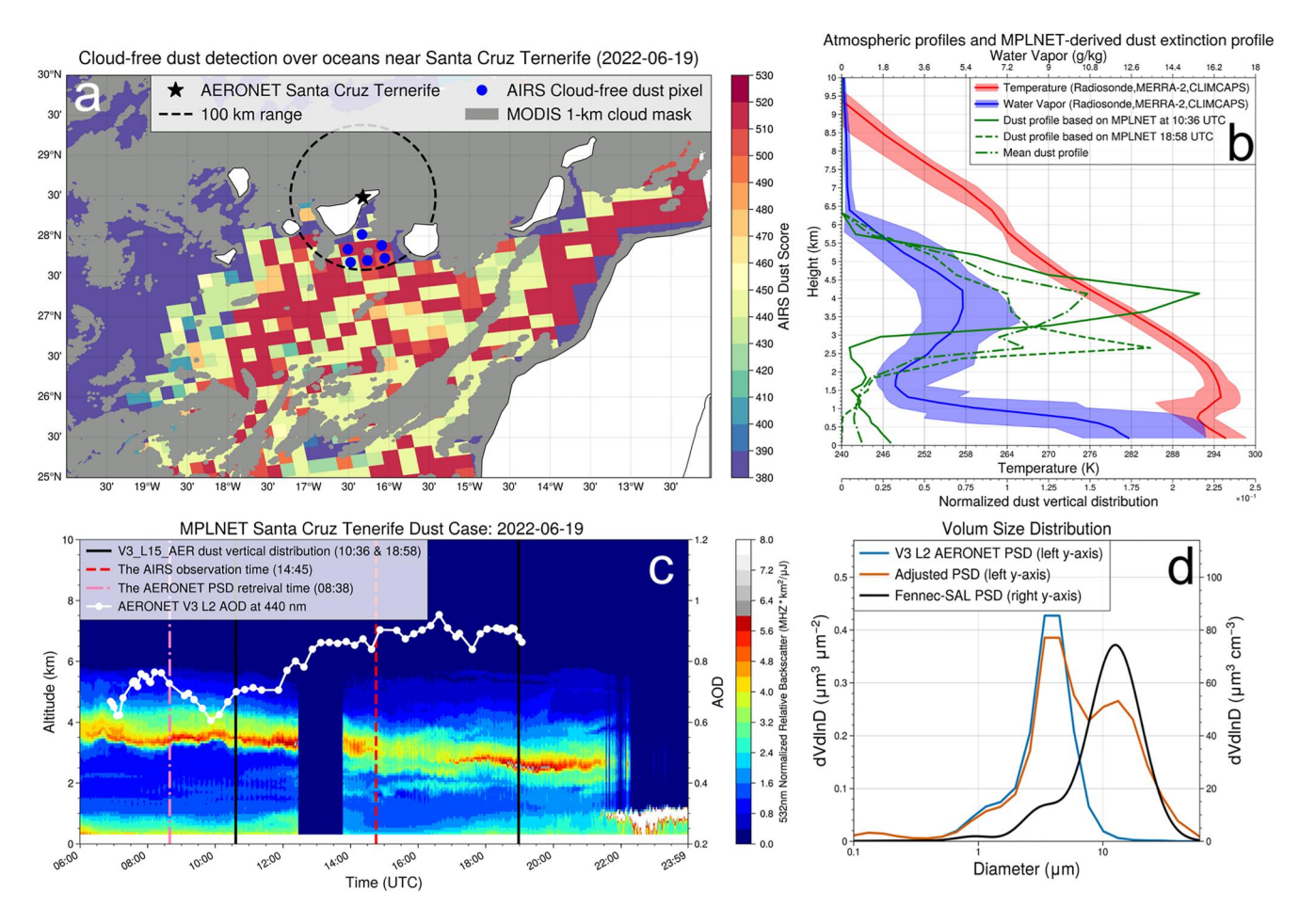


**Figure 1.** The dust case on 19 June 2022. (a) The selected AIRS pixels (blue dots) within 100 km (black dashed circle) of the AERONET SCT site (black star), with dust scores (color-filled contour pixels) >380 and without contamination by clouds indicated by MODIS cloud masks (gray masks). (b) Profiles of the mean atmospheric temperature (red solid curve) and water vapor mixing ratio (blue solid curve) from IGRA radiosondes at SCT, CLIMCAPS retrievals with retrieval errors and AIRS-collocated MERRA-2 diurnal profiles (red and blue shadow areas). The estimated dust vertical distributions from the MPLNET V3 L15 aerosol product at 10:36 UTC (green solid curve), 18:58 UTC (green dashed curve), and the corresponding mean profile (green dashed dot curve). (c) The MPLNET V3 L1 normalized relative backscatter at 532 nm from 06:00 to 24:00 UTC. The black solid, red dashed and pink dash-dotted lines indicate the observation times of the two MPLNET dust profiles, AIRS pixels and the AERONET PSD retrieval, respectively. The white dotted curve represents the time series of AERONET V3 L2 AOD at 440 nm. (d) AERONET V3 L2 Inversion dust PSD (blue curve) and the adjusted dust PSD (red curve) with a super-coarse mode referenced by the Fennec-SAL in situ vertically averaged PSD (black curve for the right y-axis).

across 2645 channels spanning 3.7–15.4  $\mu$ m at a spectral resolution of  $\lambda/\Delta\lambda \sim 1,200$  with noise equivalent delta temperature (NEDT) within 0.5 K at 250 K scenes in the TIR window region (i.e., 8–13  $\mu$ m) (Aumann et al., 2003). In particular, we select five AIRS L1C channels (i.e., 822.743, 843.913, 899.965, 965.43, and 1129.574 cm<sup>-1</sup>) principally sensitive to dust extinction while minimizing atmospheric gaseous absorption effects (e.g., water vapor and carbon dioxide) at 8–13  $\mu$ m, to assess the TIR radiative closure (DeSouza-Machado et al., 2010; Peyridieu et al., 2010). Moreover, we leverage the dust score from the AIRS L2 product for identifying dust-affected observations around AERONET at SCT (DeSouza-Machado et al., 2010). However, TIR radiative transfer simulation over the SCT island faces large uncertainty due to complex land surface properties (e.g., spatial heterogeneity and complicated spectral emissivity). For this reason, we select the AIRS pixels over the ocean surface close to SCT (see Figure 1a) for our TIR radiative closure study.

#### 2.2. Dust Vertical Distributions and TIR Refractive Index

In addition to AOD and PSD, dust vertical distribution and the TIR CRI critically influence TIR radiative signature, necessitating robust constraints (Capelle et al., 2014; DeSouza-Machado et al., 2006). The lidar observation is so far considered the most accurate way to obtain aerosol vertical structures. The NASA Micro-

ZHENG ET AL. 3 of 12

Pulse Lidar Network (MPLNET) is a global federated network of lidars collocated with AERONET sites that provides retrievals of aerosol backscatter, extinction, depolarization ratio (DPR) profiles and the column-averaged lidar ratio, using the collocated AERONET AOD as a constraint in the Fernald solution (Welton et al., 2000, 2001, 2018). This study utilizes the latest MPLNET V3 Level-1.5 (L15) quality-assured aerosol attenuated backscatter coefficients and DPR profiles at SCT for the dust case.

Because AERONET-retrieved dust properties inherently achieve radiative closure with observed sky radiances in VIS-NIR, this study focuses on TIR closure, requiring extensions of AERONET optical properties via specifications of TIR CRI. Thus, we utilize a database that contains 19 dust longwave CRIs derived from natural aerosol samples from eight major source regions globally (Di Biagio et al., 2017) (referred to as "Di-Biagio Database"). First, the Di-Biagio Database facilitates assumptions of regionally representative CRIs by tracing back the dust plume's transport paths. In addition, the CRI uncertainty can be approximated by incorporating all potential CRIs in the TIR closure assessments.

#### 2.3. Surface Properties and Atmospheric Profiles

A faithful radiative transfer simulation of TIR BT at TOA requires accurate estimates of surface and atmospheric thermodynamic properties. For better temporal matching with AIRS observations, we use the collocated AIRS-retrieved atmospheric profiles (i.e., temperature, water vapor and ozone) from the L2 Community Long-term Infrared Microwave Combined Atmospheric Processing System (CLIMCAPS) with the associated retrieval errors. The cloud-clearing process of CLIMCAPS guarantees the quality of atmospheric sounding (indicated by QC flags in the L2 product) to be free from cloud and dense aerosol interference, including dust-laden scenes (Smith & Barnet, 2023). To account for temporal variability of the atmospheric state in our simulations, we use the  $0.5^{\circ} \times 0.625^{\circ}$  gridded 3-hourly instantaneous profiles from MERRA-2 and the twice-daily (00:00 and 12:00 UTC) radiosondes at SCT, which are part of the Integral Global Radiosonde Archive (IGRA) version 2.2 (Durre et al., 2018).

Note that The CLIMCAPS surface temperature retrieval is a separate step from the atmospheric retrieval and can be negatively impacted by cloud and aerosol contaminations. Therefore, we instead acquired the  $0.01^{\circ}$  latitude  $\times$   $0.01^{\circ}$  longitude gridded daily foundation SST from the Group of High Resolution Sea Surface Temperature (GHRSST) Multiscale Ultrahigh Resolution (MUR) Level 4 (L4) product (Chin et al. (2017). The high-spatial resolution of GHRSST enables an accurate collocation with the AIRS footprints, but it does not account for SST diurnal variation. Although the effect is small for tropical oceans, we nevertheless account for the diurnal variability of SST by collocating the hourly surface skin temperature from the  $0.5^{\circ} \times 0.625^{\circ}$  gridded data of the Modern-Era Retrospective Analysis for Research and Applications Version 2 (MERRA-2; details in Gelaro et al. (2017)) and the  $0.5^{\circ} \times 0.5^{\circ}$  gridded data of the fifth-generation European Centre for Medium-Range Weather Forecasts (ECMWF) atmospheric reanalysis of the global climate (ERA5; details in Hirahara et al. (2016)). For the TIR sea surface emissivity (SSE) we adopt the model developed by Masuda et al. (1988) specified to the AIRS viewing angles.

#### 2.4. Scattering Calculations and Radiative Transfer Model Simulations

Because dust particles are non–spherical (Saito et al., 2021; Yang et al., 2007), AERONET retrievals used a spheroidal model as a computationally sufficient first-order surrogate of dust particle behavior in light-scattering computation (Dubovik et al., 2006). Therefore, the scattering properties of spheroidal dust particles are needed in this study to compare VIS-NIR results with AERONET and simulate TIR BT. Here, we use the invariant-imbedding T-matrix (IITM) method (Bi et al., 2013; Johnson, 1988) to calculate the single-particle extinction efficiency ( $Q_{\text{ext}}$ ) and cross-section ( $\sigma_{\text{ext}}$ ), single scattering albedo (SSA) and asymmetry factor (g-factor) of spheroidal dust with various aspect ratios based on inputs of dust CRI. Afterward, we calculate the bulk properties by integrating the single-scattering properties of individual particles with the given dust PSD and the size-independent aspect ratio distribution from Dubovik et al. (2006).

To simulate hyperspectral TIR BTs that are comparable with AIRS, we apply the line-by-line radiative transfer model (LBLRTM (Clough et al., 1992; Clough et al., 2005)) for precise calculations of atmospheric gaseous absorptions (e.g., water vapor handled by the MT\_CKD continuum model (Mlawer et al., 2012)) in TIR. We then couple LBLRTM-computed gaseous optical depths with dust bulk optical properties, serving as inputs for the discrete ordinate method radiative transfer (DISORT; (Stamnes et al., 1988) model to ultimately calculate TIR

ZHENG ET AL. 4 of 12



## **Geophysical Research Letters**

10.1029/2023GL106808

BTs at TOA account for dust. The combined LBLRTM-DISORT model (referred to as LBLDIS) has been widely applied for accurate aerosol and cloud radiative transfer in TIR (Turner, 2005; Wang et al., 2013). Note that the LBLDIS-simulated monochromatic BTs are convolved to AIRS channels for further comparisons (Gaiser et al., 2003).

# 3. Examination of AERONET Coarse-Mode Size Distribution Through a Case Study at Santa Cruz Tenerife on 19 June 2022

In this section, we present the implementation of the TIR radiative closure based on the AERONET VIS-NIR dust properties through a case study at AERONET SCT site on 19 June 2022 (the black star indicated in Figure 1a), which observed a dust plume (evidenced by MPLNET and AIRS; see Section 3.2) originated from North Africa indicated by the back trajectories of the NOAA Hybrid Single-Particle Lagrangian Integrated Trajectory model (HYSPLIT) (Stein et al., 2015). The AERONET-retrieved aerosol properties in this case are, thus, considered as dust properties.

#### 3.1. Sanity Check of Radiative Closure in VIS-NIR

In the first step of the radiative closure procedure, we collect the dust volume PSD (blue curve in Figure 1d) and optical properties, including spectral AODs, CRI, SSA and phase functions (green curves in Figures 2a–2c), from AERONET Inversions at SCT at 08:38:43 UTC on 19 June 2022. These data are used to assess the use of the IITM scattering calculations in the present analysis. In particular, the VIS-NIR IITM-calculated bulk dust properties (blue curves in Figures 2a–2c) are compared with those from the original AERONet algorithm. We found that the IITM-calculated dust properties agree with that from AERONET with differences mostly within their inherent uncertainty range, which are 0.01 for AOD (Eck et al., 1999), 0.03 for SSA (Sinyuk et al., 2020) and 5% residual of the phase functions at 440 nm (Dubovik et al., 2002) for scattering angles between 3° and 150° (the range for retrieval of non-spherical properties (Dubovik et al., 2006). Similar agreements of phase functions at the other three wavelengths (Figure S2 in Supporting Information S1) are found. The results demonstrate the capability of the IITM code to reproduce the AERONET retrievals, which is a prerequisite for subsequent TIR radiative closure in Section 3.2. The residuals in IITM-calculated dust properties may stem from inherent differences between the IITM code and official scattering calculations in the AERONET V3 Inversion products.

#### 3.2. Radiative Closure in TIR Based on AERONET-Retrieved Dust PSD

In the second step, we examine the TIR radiative closure by comparing the forward-simulated hyperspectral BT using the AERONET V3 L2 AOD and Inversion products with the collocated AIRS BT. To this end, we first collocated AIRS cloud-free dust-laden pixels with AERONET. As shown in Figure 1a, the Aqua MODIS 1-km cloud mask (MYD06; (Platnick et al., 2017)) is used to exclude the AIRS 13.5-km pixels that are contaminated by sub-pixel clouds (gray masks). The cloud-free pixels with AIRS dust score greater than 380 are further identified as confident dust-laden pixels (DeSouza-Machado et al., 2010). Afterward, six of the AIRS cloud-free dust-laden pixels within 100 km from SCT are selected (blue dots in Figure 1a). The spectral TIR BTs from these pixels are then used as the benchmark to compare with the LBLDIS simulations based on the necessary inputs, which are TIR dust bulk optical properties, vertical distributions, and ambient atmospheric and surface characteristics.

For dust TIR optical properties, we use the IITM to compute TIR bulk  $Q_{ext}$ , SSA and g-factor based on dust TIR CRIs, dust PSDs and spheroidal aspect ratios. Here, dust TIR CRI is determined based on the source regions estimated by the HYSPLIT model-ensemble back trajectories (Figure S3 in Supporting Information S1) initialized at the central heights of two MPLNET observed dust layers (green curves in Figure 1b) over SCT, respectively. As shown in Figure S3 in Supporting Information S1, the two groups of back trajectories indicate mixed provenance of Sahara and Sahel of the observed dust plume. Thus, we further use all eight CRIs over Sahara and Sahel from the Di-Biagio Database as the a priori TIR CRIs for the dust optical properties calculation. We note that the AERONET PSD (blue curve in Figure 1d) is column-integrated. Thus, although the vertical variation of particle size is generally homogenous (Ryder et al., 2013, 2019), we assume a vertical variation of dust PSD referencing the in situ measured Fennec Saharan Air Layer (SAL) dust PSD (Ryder et al., 2013; details in Supporting Information S1 and Figure S4), which was also measured over areas of Canary Islands with similar

ZHENG ET AL. 5 of 12

1944/8007, 2024, 4, Downloaded from https://agupubs.onlinelibrary.wiley.com/doi/10.1029/2023GL106808, Wiley Online Library on [18/02/2024]. See the Terms and Conditions (https://onlinelibrary.wiley.com/terms-and-conditions) on Wiley Online Library for rules of use; OA articles are governed by the applicable Creative Commons Licenses

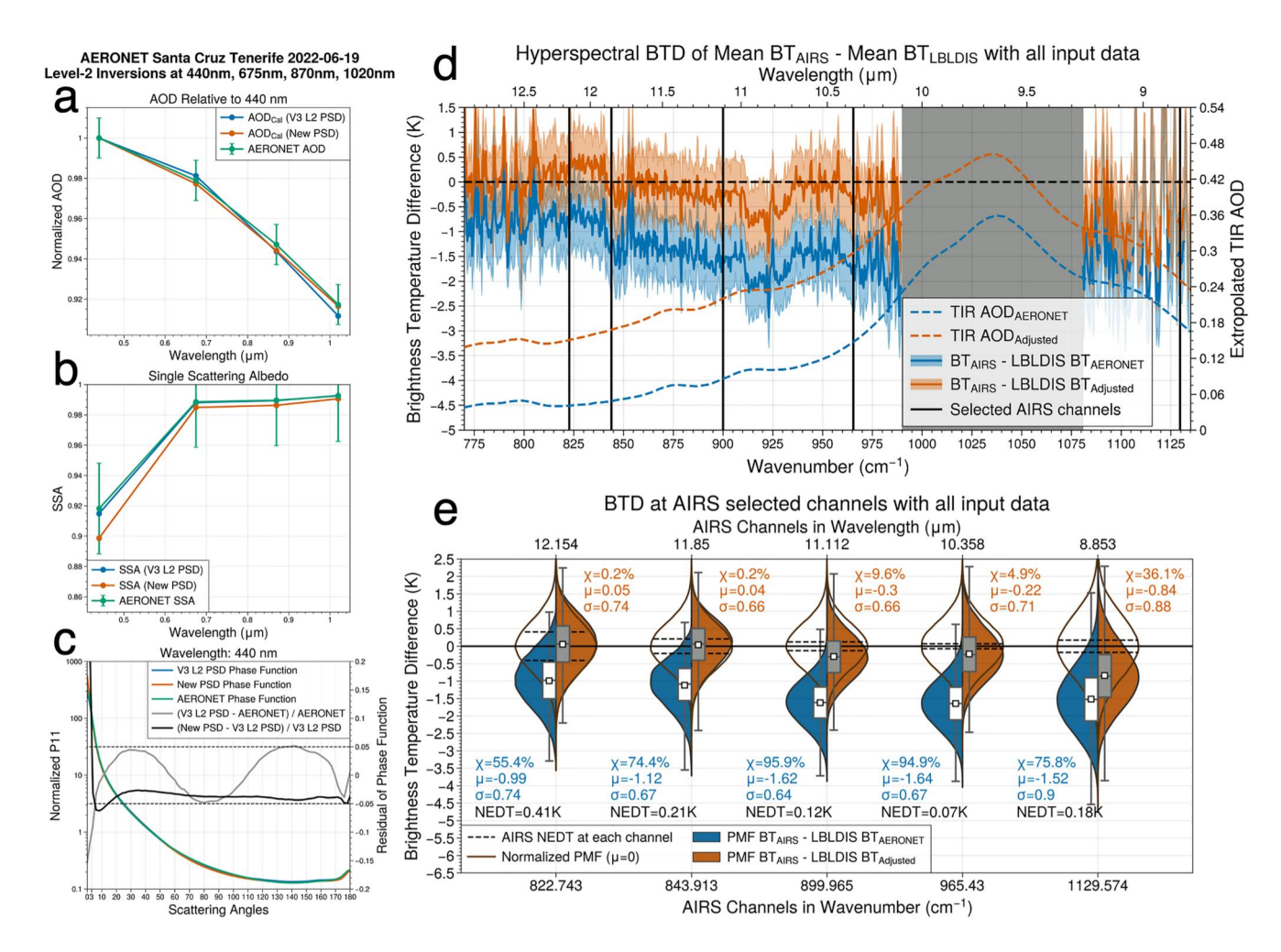


Figure 2. Dust spectral AOD normalized to 440 nm (a), SSA (b), phase functions (left y-axis in c) and residuals (gray and black curves for the right y-axis in c) at 440 nm from AERONET V3 L2 Inversions (a–c, green) and IITM calculations based on the AERONET V3 L2 PSD (a–c, blue) and the adjusted dust PSD (a–c, red). (d) The mean spectral BTDs (AIRS BT—LBLDIS BT; real curves with respect to the left y-axis) from 770 to 1,130 cm<sup>-1</sup> simulated using extrapolated TIR AODs (dash curves with respect to the right y-axis) based on AERONET PSD (blue) and the adjusted PSD (red), and other reference inputs indicated in Section 3.1. The gray mask represents the ozone absorption spectral regime. (e) The violin and box plots of the distribution of BTDs at the five selected AIRS channels based on AERONET PSD (blue violins, white box) and the adjusted PSD (red violins, gray box). The box boundaries and whiskers represent the 25th and 75th percentiles, and the minimum and maximum of BTDs, respectively. The χ, μ and σ represent the bias, mean and standard deviation. The brown curves represent the normalized PMF with  $\mu = 0$  and the same σ as BTD distributions. The black dashed lines represent the range of AIRS NEDTs at the five channels that are listed as black texts.

source regions from North Africa. It indicates the possibility of our case to have similar vertical distribution dust PSD. Afterward, we extrapolate the temporally-matched AERONET AOD at 440 nm (AOD<sub>440nm</sub>) from the directly measured AERONET AOD product at 14:52 UTC (white dotted curve in Figure 1c) to TIR spectrum based on the  $Q_{\rm ext}$  ratio between VIS and TIR as AOD<sub> $\lambda$ </sub> =  $AOD_{440nm} \cdot Q_{\rm ext}$ ,  $\lambda/Q_{\rm ext}$ , where  $\lambda$  is the wavelength of 8–13 µm. In the next step, we need the dust vertical distribution to scale AOD<sub> $\lambda$ </sub> vertically into layer extinction coefficients in LBLDIS.

The dust vertical distribution is specified using the collocated MPLNET L15 aerosol backscatter and DPR profile retrievals using the method from Yu et al. (2015) (details in Supporting Information S1). Although the MPLNET L1 relative backscatter profiles are available for most of the day (background color-filled contours in Figure 1c), only two L15 aerosol profile retrievals are available at 10:36 and 18:58 UTC (black solid lines), respectively, which have spatiotemporal offsets with respect to the 100-km range AIRS observations (14:45 UTC; red dashed line) and AERONET PSD (08:38 UTC, pink dash-dotted line). However, it is reasonable to assume a limited variation of dust PSD within several hours for a dust plume with the age of 2 days estimated by HYSPLIT models (Figure S3b in Supporting Information S1) (Ryder et al., 2019). Moreover, the dust plume height at 14:45 UTC

ZHENG ET AL. 6 of 12

indicated by the time series of the L1 backscatter profile is in between the two L15 backscatter profiles. Accordingly, we average the two L15 dust profiles as a proxy for dust vertical distribution at the AIRS observation time and consider the difference among the three profiles as the uncertainty due to the spatiotemporal variations of dust vertical distributions at the selected AIRS pixels.

For the atmospheric profiles, as introduced in Section 2.3, we obtained two timely matched collocated CLIAMCAPS atmospheric profiles with the best QC flag, two 12-hourly radiosondes at over SCT, and eight collocated 3-hourly MERRA-2 profiles on 19 June 2022, as shown in Figure 1b. The associated variations and errors among these profiles (shadow areas in Figure 1b) are used to represent the corresponding uncertainties. The SST is represented by the averaged value (294.5 K) from the AIRS-collocated grids of GHRSST, hourly MERRA-2 and ERA5 at 15:00 UTC (see Figure S1 in Supporting Information S1) with uncertainty characterized by the 0.358 K standard deviation among the grid cells. In addition, as the diurnal variability of the skin temperature from MERRA-2 and ERA5 is up to 0.6 K (Figures S1d and S1e in Supporting Information S1), we assumed a 1 K error to account for the temporal mismatch between SST data sets and AIRS observations. Finally, we calculated the mean TIR SSE at the viewing angles of six selected AIRS pixels based on Masuda et al. (1988) and assigned an estimated error of 0.004 according to previous in situ measurements (Konda et al., 1994; Niclòs et al., 2005).

In summary, we have three vertical dust profiles, 16 atmospheric profiles (six from two CLIMCAPS  $\pm$  retrieval errors; two from 12-hourly radiosondes, eight from 3-hourly MERRA-2), eight groups of dust TIR bulk properties, five SSTs (SST  $\pm$  0.358K and  $\pm$ 1K) and three spectral SSEs (SSE  $\pm$  0.004), as the inputs for the LBLDIS simulation. Consequently, we implement 5,760 LBLDIS simulations of TIR spectral BTs at TOA to compare with each of the six AIRS pixels. In total, we have 34,560 BT differences (BTDs) between AIRS BTs and LBLDIS-simulated BTs to quantify the radiative closure in TIR. Specifically, the variation of the BTDs represents the overall uncertainty due to the variations of input data sets other than dust PSD, including dust TIR CRI, vertical profiles, surface, and atmospheric thermodynamic states. It may not be an exhaustive list while it should cover the most important sources of uncertainties.

As shown in Figure 2d, the mean spectral BTDs (AIRS BT—LBLDIS BT) in 770–1,130 cm $^{-1}$  (8.8–13 µm) averaged by the 34,560 BTDs with uncertainties represented by the standard deviation ( $\sigma$ ) of the BTDs. With the AERONET PSD and VIS-NIR CRIs, the simulated BTs are systematically warmer than AIRS BTs, leading to negative BTDs (blue solid curve in Figure 2d). The warm bias exhibits V-shaped spectral behavior, likely due to the underestimated dust extinction (Clarisse et al., 2019; DeSouza-Machado et al., 2010; Pierangelo et al., 2004). Notably, the upper limit of BTD  $\sigma$  for the blue curve in the dust-sensitive spectrum (850–990 cm $^{-1}$ ) remains above 0.5 K, which indicates a likelihood that dust microphysical properties are suspectable in the simulation.

To statistically analyze the TIR radiative closure, we present the BTD distributions as violin and box plots (blue violins and white boxes in Figure 2e) at five dust-sensitive AIRS channels (see Section 2.1). The white boxes in Figure 2e at the five channels indicate over 75% of negative BTDs. It means that over 75% of the simulated BTs based on AERONET inputs are warmer than AIRS BTs. We further define a systematic bias index  $\chi$  as  $\chi = (1 - P_{\rm BTD}/P_{\rm ZERO}) \times 100\%$ , where  $P_{\rm BTD}$  is the probability of the BTD samples falling within the range of 0 ± AIRS NEDT according to the probability mass function (PMF);  $P_{\rm ZERO}$  is the corresponding probability if the BTD PMF were shifted with the mean to zero and the  $\sigma$  kept same. As such, if  $P_{\rm BTD} = P_{\rm ZERO}$ , the  $\chi = 0$ , which means the simulated BTs have no systematic bias but only random uncertainties. A  $P_{\rm BTD} = 0$  means that none of the simulated BT is able to match the corresponding AIRS BT, leading to  $\chi = 100\%$  (Details in Supporting Information S1).

The blue violins show  $\chi$  from 55.4% (1129.574 cm<sup>-1</sup>) to 95.9% (899.965 cm<sup>-1</sup>) among the five channels, indicating a consistent warm bias in the simulated BTs compared with AIRS BT. In particular, the  $\chi$  can reach 95% for the channel at 899.965 cm<sup>-1</sup> that has the higher dust extinction represented by the spectral AOD (dashed curves in Figure 2d), suggesting that the current set of AERONET retrievals of dust has a limited capacity to close the TIR. One possible reason is that the dust optical properties in TIR, in particular AOD (blue dashed curve in Figure 2d) extrapolated based on the AERONET-retrieved dust properties, have too little "effective absorption" (i.e., absorption + backward scattering (Garnier et al., 2012; Pavolonis et al., 2013)) to reduce outgoing radiance with BT as cold as AIRS-observed BT at TOA (Osborne et al., 2011). This opens us to the possibility that the AERONET-retrieved coarse-mode PSD is too fine to have enough extinction in TIR, which will be tested in the next section.

ZHENG ET AL. 7 of 12

#### 3.3. Radiative Closure in VIS-NIR and TIR Based on the Adjusted Dust PSD With a Super-Coarse Mode

Based on the above results, we hypothesize that adding a super-coarse mode to the AERONET retrieved dust PSD (Figure 1d) would improve the TIR radiative closure while having limited impacts on the VIS-NIR closure. To test this assumption, in this section, we revisit the VIS-NIR radiative closure by adjusting the AERONET coarsemode PSD with all other variables fixed.

Specifically, we introduce a super-coarse mode to the AERONET retrieved PSD (blue curve in Figure 1d) based on the third lognormal mode of the log-fitted in situ measured Fennec SAL dust PSD (black curve in Figure 1d; details in Ryder et al. (2019)). The new PSD (red curve in Figure 1d) is normalized to have the same total dust surface area as the AERONET-retrieved PSD to keep the total projected area conserved. As such, if the two PSDs have similar  $Q_{\rm ext}$ , so do their corresponding AODs because AOD is the product of  $Q_{\rm ext}$  and total projected area.

As shown in Figure 2a, the spectral AOD corresponding to the new PSD has limited changes within the 0.01 AERONET AOD uncertainty. Moreover, the differences in SSA are also within the AERONET inversion uncertainty of 0.03 (red curve and green error bars in Figure 2b). In Figure 2c, although more super-coarse particles substantially increase bulk forward scattering, represented by the enhanced near-forward (<3°) phase functions (black curves in Figure 2c; Figure S2 in Supporting Information S1), changes from 3° to 150° are mostly within the acceptable 5% residuals indicated in AERONET Inversions (Dubovik et al., 2002). All together, these results suggest that introducing an extra super-coarse mode has negligible impact on the AERONET-retrieved dust properties in VIS-NIR. From a different perspective, it also means that the current AERONET retrieval algorithms have little sensitivity to super-coarse mode dust.

Using the adjusted, coarser PSD, we revisit the TIR radiative closure with other variables fixed as in Figures 2d and 2e in Section 3.2. The simulated BT better match with AIRS this time as the BTDs shifts up 1–1.5 K for channels with wavelength greater than 10  $\mu$ m, approaching zero differences (red solid curve in Figure 2d). The  $\chi$  indices of the BTD distributions at the five AIRS channels using the adjusted PSD (red violins and gray boxes in Figure 2e) are significantly reduced, for instance, from 74.4% to 0.2% at 843.913 cm<sup>-1</sup> (11.85  $\mu$ m) and from 94.9% to 4.9% at 965.43 cm<sup>-1</sup> (10.36  $\mu$ m), compared to that using the AERONET PSD. The increased BTDs mainly result from a large increase of the extrapolated TIR DOD, by almost a factor of 3, due to the greater volume of super-coarse particles (red dashed curve in Figure 2d), as extinction grows significantly with coarse mode size at TIR wavelengths (Pierangelo et al., 2005; Ryder et al., 2019; Zheng et al., 2023). Note that 36% bias remains at the channel of 1129.574 cm<sup>-1</sup> (8.85  $\mu$ m) where dust TIR CRI has a large variability (Di Biagio et al., 2017). Nonetheless, compared with the result based on AERONET-retrieved dust PSD in Section 3.1, it is evident that with the coarser dust PSD, the probability of closing the bias is remarkably increased, although achieving the closure needs an optimal combination among all of the dust properties and thermodynamic states, which is beyond this study.

#### 4. Discussion and Conclusions

This study performs radiative closure assessments from VIS-NIR to TIR for an AERONET-observed Saharan dust case. Simulated TIR BT, based on AERONET-retrieved PSD, systematically appears warmer than collocated AIRS observations. Theoretically, the warm bias can be corrected by improving the combination of dust properties and thermodynamic profiles, all of which the AIRS instrument is sensitive to. However, in this study, the DOD and dust vertical extent were carefully constrained via the AERONET measurement and MPLNET retrieval, while the use of collocated atmospheric profiles and SSTs from various data sets assures us that we cover the most appropriate thermodynamic states. Therefore, this study demonstrates a new perspective that introducing a super-coarse mode to the AERONET-retrieved PSD can help reduce warm biases in the TIR while minimally affecting the VIS-NIR retrievals. These results support the hypothesis that AERONET has limited sensitivity to the super-coarse mode dust particles with  $D_p > 10~\mu\text{m}$ , which are crucial in determining the radiative properties of dust in the TIR and dominate the contributions to suspended dust mass. However, these findings do not indicate any flaws in the AERONET inversion method. In turn, they highlight potential improvements for retrieval of dust properties, particularly the full PSD range, by using synergies between VIS-NIR and TIR observations.

This study has several limitations, including imperfect spatiotemporal collocations among observational data sets. Quality-assured AERONet almucantar retrievals require solar zenith angles (SZA) above 50°, causing time

ZHENG ET AL. 8 of 12

#### Acknowledgments

J. Zheng, Z. Zhang and A. Garnier are supported by a NASA grant (no. 80NSSC20K0130) from the CALIPSO and CloudSat program managed by David Considine. Z. Zhang also acknowledges funding support from the NSF (AGS-2232138). H. Yu was supported by the CloudSat/CALIPSO program. C. L. Ryder acknowledges funding from NERC IRF Grant NE/M018288/1. The computations in this study were performed at the UMBC High Performance Computing Facility (HPCF). The facility is supported by the US National Science Foundation through the MRI program (Grants CNS-0821258 and CNS-1228778) and the SCREMS program (Grant DMS-0821311), with substantial support from UMBC. We thank NASA for providing the AIRS, CLIMCAPS and MODIS data, which are publicly available at https://disc.gsfc.nasa. gov/ and https://ladsweb.modaps.eosdis. nasa.gov/. We thank the AERONET and MPLNET project at NASA/GSFC funded by the NASA Radiation Sciences Program and Earth Observing System, for providing the ground-based aerosol data, which are publicly available at https://aeronet.gsfc. nasa.gov/ and https://mplnet.gsfc.nasa. gov/download\_tool. AERONET sun photometer at Santa Cruz was calibrated through the AEROSPAIN Central Facility (https://aerospain.aemet.es/) supported by the European Community Research Infrastructure Action under the ACTRIS grant agreement no. 871115. The IITM light-scattering computational model used in this study was developed by Dr. Ping Yang's group at Texas A&M University. The laboratory experiments to retrieve the dust refractive indices in Di Biagio et al. (2017) that feed this work had received funding from the European Union's Horizon 2020 research and innovation program through the EUROCHAMP-2020 Infrastructure Activity under grant agreement no. 730997. They were supported by the French national programme LEFE/INSU (Les Enveloppes Fluides et l'Environnement/Institut National des Sciences de l'Univers) and by the OSU-EFLUVE (Observatoire des Sciences de l'Univers-Enveloppes Fluides de la Ville à l'Exobiologie) through dedicated research funding to the RED-DUST project. The authors acknowledge the CNRS-INSU for supporting the CESAM chamber as a national facility as part of the French ACTRIS Research Infrastructure as well as the AERIS data center (www.aeris-data.fr) for distributing and curing the data produced by the CESAM chamber through the hosting of the EUROCHAMP datacenter (data.eurochamp.org). C. D. Biagio was supported by the Centre National des Etudes Spatiales (CNES) and by the CNRS via the Labex L-IPSL, which is funded by the ANR (Grant ANR-10-LABX-0018).

offsets with polar-orbit satellite observations over mid-to-low latitude dust regions, which typically have SZA < 30°, especially in high-dust-activity seasons (spring and summer) (Sinyuk et al., 2020). Furthermore, the over-ocean requirement for the TIR radiative closure at TOA also deviates the qualified AIRS pixels 50-100 km from the AERONET geolocation. Lastly, the studied case lacks coincident in situ measured dust PSDs for precise references. Hence, further attempts at radiative closures for more cases with collocated in situ measurements are recommended to strengthen the results of the present work and support its applicability. Ultimately, including ground-based TIR instruments along with the VIS-NIR sun-photometers at the dust-dominated AERONET sites could be highly beneficial to overcome the abovementioned limitations and improve the retrieval of dust properties.

#### **Data Availability Statement**

The AIRS L1C data is available from AIRS Science Team/Larrabee Strow (2019). The CLIMCAPS L2 data can be found in Chris Barnet (2020). The AERONET Version 3 Level 2 AOD data and Inversion data from the AERONET website (https://aeronet.gsfc.nasa.gov, last access: 19 January 2024; Giles et al. (2019)) and the website provides these data freely to the public. Data may be acquired by utilizing several download mechanisms including site-by-site download tools. For instance, click "download tool" and select "Santa\_Cruz\_Tenerife" then choose the date to be "19 June 2022" to further select the corresponding AOD data. The MPLNET L15 Aerosol Data is publicly available on the MPLNET website (https://mplnet.gsfc.nasa.gov, last access: 19 January 2024; Welton et al. (2018)). Data may be acquired by utilizing several download mechanisms including site-by-site download tools, with procedures similar to AERONET data. The IGRA radiosonde data is publicly available on the IGRA website (https://www.ncei.noaa.gov/products/weather-balloon/integrated-global-radiosondearchive, last access: 19 January 2024; Durre et al. (2018)). Data may be acquired by utilizing several download mechanisms including site-by-site download tools. For instance, click "Sounding Data Format" to look up the site ID for "TENERIFE-GUIMAR." Then, click "HTTPS: All Sounding Data" under "Sounding Data" and download the file with the corresponding site ID. The MERRA-2 hourly skin temperature is from "MERRA2\_400. inst1\_2d\_asm\_Nx.20220619.nc4" and is available at Gelaro et al. (2017) and can be downloaded at Global Modeling and Assimilation Office (GMAO) (2015a). The MERRA-2 3-hourly atmospheric profiles are from "MERRA2\_400.inst3\_3d\_asm\_Nv.20220619.nc4" and are available at Gelaro et al. (2017) and can be downloaded at Global Modeling and Assimilation Office (GMAO) (2015b). The GHRSST MUR L4 foundation SST can be found at JPL MUR MEaSUREs Project. (2015). The ERA5 hourly skin temperature can be found by Hirahara et al. (2016) and downloaded at Hersbach et al. (2023). The Fennec-SAL dust particle size distribution is provided by Dr. Claire L. Ryder at University of Reading (c.l.ryder@reading.ac.uk), which is publicly available in the Supplement in Ryder et al. (2019). The eight TIR dust complex refractive indices over Sahara and Sahel are provided by Dr. Claudia Di Biagio at the Université Paris Cité and Univ Paris Est Creteil, CNRS, LISA (cdibiagio@lisa.ipsl.fr), which are available in the Supplement in Di Biagio et al. (2017).

#### References

Adebiyi, A., Kok, J. F., Murray, B. J., Ryder, C. L., Stuut, J.-B. W., Kahn, R. A., et al. (2023). A review of coarse mineral dust in the Earth system. Aeolian Research, 60, 100849. https://doi.org/10.1016/j.aeolia.2022.100849

AIRS Science Team/Larrabee Strow. (2019). AIRS/Aqua L1C infrared (IR) resampled and corrected radiances V6.7, Greenbelt, MD, USA [Dataset]. Goddard Earth Sciences Data and Information Services Center (GES DISC). https://doi.org/10.5067/VWD3DRC07UEN

Aumann, H. H., Chahine, M. T., Gautier, C., Goldberg, M. D., Kalnay, E., McMillin, L. M., et al. (2003). AIRS/AMSU/HSB on the Aqua mission: Design, science objectives, data products, and processing systems. IEEE Transactions on Geoscience and Remote Sensing, 41(2), 253-264. https://doi.org/10.1109/tgrs.2002.808356

Barnet, C. (2020). Sounder SIPS: AQUA AIRS IR-only level 2 CLIMCAPS: Cloud cleared radiances V2, Greenbelt, MD, USA [Dataset]. Goddard Earth Sciences Data and Information Services Center (GES DISC), https://doi.org/10.5067/9RRS80QCT0E9

Bi, L., Yang, P., Kattawar, G. W., & Mishchenko, M. I. (2013). Efficient implementation of the invariant imbedding T-matrix method and the separation of variables method applied to large nonspherical inhomogeneous particles. Journal of Quantitative Spectroscopy and Radiative Transfer, 116, 169-183. https://doi.org/10.1016/j.jqsrt.2012.11.014

Capelle, V., Chédin, A., Siméon, M., Tsamalis, C., Pierangelo, C., Pondrom, M., et al. (2014). Evaluation of IASI-derived dust aerosol characteristics over the tropical belt. Atmospheric Chemistry and Physics, 14(17), 9343-9362. https://doi.org/10.5194/acp-14-9343-2014

Chin, T. M., Vazquez-Cuervo, J., & Armstrong, E. M. (2017). A multi-scale high-resolution analysis of global sea surface temperature. Remote Sensing of Environment, 200, 154-169. https://doi.org/10.1016/j.rse.2017.07.029

Choobari, O. A., Zawar-Reza, P., & Sturman, A. (2014). The global distribution of mineral dust and its impacts on the climate system: A review. Atmospheric Research, 138, 152-165. https://doi.org/10.1016/j.atmosres.2013.11.007

Clarisse, L., Clerbaux, C., Franco, B., Hadji-Lazaro, J., Whitburn, S., Kopp, A. K., et al. (2019). A decadal data set of global atmospheric dust retrieved from IASI satellite measurements. Journal of Geophysical Research: Atmospheres, 124(3), 1618-1647. https://doi.org/10.1029/ 2018jd029701

ZHENG ET AL. 9 of 12



## **Geophysical Research Letters**

- 10.1029/2023GL106808
- Clough, S. A., Iacono, M. J., & Moncet, J.-L. (1992). Line-by-line calculations of atmospheric fluxes and cooling rates: Application to water vapor. *Journal of Geophysical Research*, 97(D14), 15761–15785. https://doi.org/10.1029/92jd01419
- Clough, S. A., Shephard, M. W., Mlawer, E. J., Delamere, J. S., Iacono, M. J., Cady-Pereira, K., et al. (2005). Atmospheric radiative transfer modeling: A summary of the AER codes. *Journal of Quantitative Spectroscopy and Radiative Transfer*, 91(2), 233–244. https://doi.org/10.1016/j.jqsrt.2004.05.058
- DeSouza-Machado, S. G., Strow, L. L., Hannon, S. E., & Motteler, H. E. (2006). Infrared dust spectral signatures from AIRS. *Geophysical Research Letters*, 33(3), L03801. https://doi.org/10.1029/2005gl024364
- DeSouza-Machado, S. G., Strow, L. L., Imbiriba, B., McCann, K., Hoff, R. M., Hannon, S. E., et al. (2010). Infrared retrievals of dust using AIRS: Comparisons of optical depths and heights derived for a North African dust storm to other collocated EOS A-Train and surface observations. *Journal of Geophysical Research*, 115(D15), D15201. https://doi.org/10.1029/2009jd012842
- Di Biagio, C., Formenti, P., Balkanski, Y., Caponi, L., Cazaunau, M., Pangui, E., et al. (2017). Global scale variability of the mineral dust long-wave refractive index: A new dataset of in situ measurements for climate modeling and remote sensing. *Atmospheric Chemistry and Physics*, 17(3), 1901–1929. https://doi.org/10.5194/acp-17-1901-2017
- Dubovik, O., Holben, B., Eck, T. F., Smirnov, A., Kaufman, Y. J., King, M. D., et al. (2002). Variability of absorption and optical properties of key aerosol types observed in worldwide locations. *Journal of the Atmospheric Sciences*, 59(3), 590–608. https://doi.org/10.1175/1520-0469(2002) 059<0590:voaaop>2.0.co;2
- Dubovik, O., Sinyuk, A., Lapyonok, T., Holben, B. N., Mishchenko, M., Yang, P., et al. (2006). Application of spheroid models to account for aerosol particle nonsphericity in remote sensing of desert dust. *Journal of Geophysical Research*, 111(D11), D11208. https://doi.org/10.1029/ 2005id006619
- Dubovik, O., Smirnov, A., Holben, B., King, M., Kaufman, Y., Eck, T., & Slutsker, I. (2000). Accuracy assessments of aerosol optical properties retrieved from Aerosol Robotic Network (AERONET) Sun and sky radiance measurements. *Journal of Geophysical Research*, 105(D8), 9791–9806. https://doi.org/10.1029/2000id900040
- Durre, I., Yin, X., Vose, R. S., Applequist, S., & Arnfield, J. (2018). Enhancing the data coverage in the integrated global radiosonde Archive. Journal of Atmospheric and Oceanic Technology, 35(9), 1753–1770. https://doi.org/10.1175/jtech-d-17-0223.1
- Eck, T. F., Holben, B. N., Reid, J. S., Dubovik, O., Smirnov, A., O'Neill, N. T., et al. (1999). Wavelength dependence of the optical depth of biomass burning, urban, and desert dust aerosols. *Journal of Geophysical Research*, 104, 31333–31349.
- Gaiser, S. L., Aumann, H. H., Strow, L. L., Hannon, S. E., & Weiler, M. (2003). In-flight spectral calibration of the atmospheric infrared sounder. IEEE Transactions on Geoscience and Remote Sensing, 41(2), 287–297. https://doi.org/10.1109/tgrs.2003.809708
- Garnier, A., Pelon, J., Dubuisson, P., Faivre, M., Chomette, O., Pascal, N., & Kratz, D. P. (2012). Retrieval of cloud properties using CALIPSO imaging infrared radiometer. Part I: Effective emissivity and optical depth. *Journal of Applied Meteorology and Climatology*, 51(7), 1407–1425. https://doi.org/10.1175/jamc-d-11-0220.1
- Gelaro, R., McCarty, W., Suárez, M. J., Todling, R., Molod, A., Takacs, L., et al. (2017). The Modern-Era Retrospective Analysis for Research and Applications, Version 2 (MERRA-2). *Journal of Climate*, 30(14), 5419–5454. https://doi.org/10.1175/jcli-d-16-0758.1
- Giles, D. M., Sinyuk, A., Sorokin, M. G., Schafer, J. S., Smirnov, A., Slutsker, I., et al. (2019). Advancements in the Aerosol Robotic Network (AERONET) Version 3 database—Automated near-real-time quality control algorithm with improved cloud screening for Sun photometer aerosol optical depth (AOD) measurements. Atmospheric Measurement Techniques, 12(1), 169–209. https://doi.org/10.5194/amt-12-169-2019
- Ginoux, P., Prospero, J. M., Gill, T. E., Hsu, N. C., & Zhao, M. (2012). Global-scale attribution of anthropogenic and natural dust sources and their emission rates based on MODIS Deep Blue aerosol products. *Reviews of Geophysics*, 50(3), RG3005. https://doi.org/10.1029/2012rg000388
- Global Modeling, & Assimilation Office (GMAO). (2015b). MERRA-2 inst3\_3d\_asm\_Nv: 3d,3-Hourly,Instantaneous,Model-Level,Assimilation,Assimilated Meteorological Fields V5.12.4 [Dataset]. Goddard Earth Sciences Data and Information Services Center (GES DISC. https://doi.org/10.5067/WWOSXO8IVFW8
- Global Modeling, & Assimilation Office (GMAO). (2015a). MERRA-2 inst1\_2d\_asm\_Nx: 2d,1-Hourly,Instantaneous,Single-Level,Assimilation,Single-Level Diagnostics V5.12.4 [Dataset]. Goddard Earth Sciences Data and Information Services Center (GES DISC). https://doi.org/10.5067/3Z173KIE2TPD
- Goudie, A. (1983). Dust storms in space and time. *Progress in Physical Geography*, 7(4), 502–530. https://doi.org/10.1177/030913338300700402 Hersbach, H., Bell, B., Berrisford, P., Biavati, G., Horányi, A., Muñoz Sabater, J., et al. (2023). ERA5 hourly data on single levels from 1940 to present [Dataset]. Copernicus Climate Change Service (C3S) Climate Data Store (CDS). https://doi.org/10.24381/cds.adbb2d47
- Hirahara, S., Balmaseda, M. A., Boisseson, E., & Hersbach, H. (2016). Sea surface temperature and sea ice concentration for ERA5 (Vol. 26). European Centre for Medium-Range Weather Forecasts.
- Holben, B. N., Eck, T. F., Slutsker, I., Tanré, D., Buis, J. P., Setzer, A., et al. (1998). AERONET—A federated instrument network and data archive for aerosol characterization. *Remote Sensing of Environment*, 66, 1–16. https://doi.org/10.1016/s0034-4257(98)00031-5
- Johnson, B. R. (1988). Invariant imbedding T matrix approach to electromagnetic scattering. *Applied Optics*, 27(23), 4861–4873. https://doi.org/10.1364/ao.27.004861
- JPL MUR MEaSURES Project. (2015). GHRSST level 4 MUR global foundation sea surface temperature analysis. Ver. 4.1 [Dataset]. JPL MUR MEaSURES Project. https://doi.org/10.5067/GHGMR-4FJ04
- Kinne, S., Schulz, M., Textor, C., Guibert, S., Balkanski, Y., Bauer, S. E., et al. (2006). An AeroCom initial assessment—Optical properties in aerosol component modules of global models. Atmospheric Chemistry and Physics, 6(7), 1815–1834. https://doi.org/10.5194/acp-6-1815-2006
- Kok, J. F., Ridley, D. A., Zhou, Q., Miller, R. L., Zhao, C., Heald, C. L., et al. (2017). Smaller desert dust cooling effect estimated from analysis of dust size and abundance. *Nature Geoscience*, 10(4), 274–278. https://doi.org/10.1038/ngeo2912
- Konda, M., Imasato, N., Nishi, K., & Toda, T. (1994). Measurement of the sea surface emissivity. *Journal of Oceanography*, 50(1), 17–30. https://doi.org/10.1007/bf02233853
- Mahowald, N., Albani, S., Kok, J. F., Engelstaeder, S., Scanza, R., Ward, D. S., & Flanner, M. G. (2014). The size distribution of desert dust aerosols and its impact on the Earth system. Aeolian Research, 15, 53–71. https://doi.org/10.1016/j.aeolia.2013.09.002
- Masuda, K., Takashima, T., & Takayama, Y. (1988). Emissivity of pure and sea waters for the model sea surface in the infrared window regions. Remote Sensing of Environment, 24(2), 313–329. https://doi.org/10.1016/0034-4257(88)90032-6
- McConnell, C. L., Highwood, E. J., Coe, H., Formenti, P., Anderson, B., Osborne, S., et al. (2008). Seasonal variations of the physical and optical characteristics of Saharan dust: Results from the dust outflow and deposition to the ocean (DODO) experiment. *Journal of Geophysical Research*, 113(D14). https://doi.org/10.1029/2007jd009606
- Mlawer, E. J., Payne, V. H., Moncet, J.-L., Delamere, J. S., Alvarado, M. J., & Tobin, D. C. (2012). Development and recent evaluation of the MT\_CKD model of continuum absorption. *Philosophical Transactions of the Royal Society A: Mathematical, Physical & Engineering Sciences*, 370(1968), 2520–2556. https://doi.org/10.1098/rsta.2011.0295

ZHENG ET AL. 10 of 12

- Müller, D., Lee, K.-H., Gasteiger, J., Tesche, M., Weinzierl, B., Kandler, K., et al. (2012). Comparison of optical and microphysical properties of pure Saharan mineral dust observed with AERONET Sun photometer, Raman lidar, and in situ instruments during SAMUM 2006. *Journal of Geophysical Research*, 117(D7), D07211. https://doi.org/10.1029/2011jd016825
- Niclòs, R., Valor, E., Caselles, V., Coll, C., & Sánchez, J. M. (2005). In situ angular measurements of thermal infrared sea surface emissivity—Validation of models. *Remote Sensing of Environment*, 94(1), 83–93. https://doi.org/10.1016/j.rse.2004.09.002
- Osborne, S. R., Baran, A. J., Johnson, B. T., Haywood, J. M., Hesse, E., & Newman, S. (2011). Short-wave and long-wave radiative properties of Saharan dust aerosol. *Quarterly Journal of the Royal Meteorological Society*, 137(658), 1149–1167. https://doi.org/10.1002/qj.771
- Pavolonis, M. J., Heidinger, A. K., & Sieglaff, J. (2013). Automated retrievals of volcanic ash and dust cloud properties from upwelling infrared measurements. *Journal of Geophysical Research: Atmospheres*, 118(3), 1436–1458. https://doi.org/10.1002/jgrd.50173
- Peyridieu, S., Chédin, A., Tanré, D., Capelle, V., Pierangelo, C., Lamquin, N., & Armante, R. (2010). Saharan dust infrared optical depth and altitude retrieved from AIRS: A focus over North Atlantic—Comparison to MODIS and CALIPSO. *Atmospheric Chemistry and Physics*, 10(4), 1953–1967. https://doi.org/10.5194/acp-10-1953-2010
- Pierangelo, C., Chédin, A., Heilliette, S., Jacquinet-Husson, N., & Armante, R. (2004). Dust altitude and infrared optical depth from AIRS. Atmospheric Chemistry and Physics, 4(7), 1813–1822. https://doi.org/10.5194/acp-4-1813-2004
- Pierangelo, C., Mishchenko, M., Balkanski, Y., & Chédin, A. (2005). Retrieving the effective radius of Saharan dust coarse mode from AIRS. Geophysical Research Letters, 32(20), L20813. https://doi.org/10.1029/2005gl023425
- Platnick, S., Meyer, K., King, M., Wind, G., Amarasinghe, N., Marchant, B., et al. (2017). The MODIS cloud optical and microphysical products: Collection 6 updates and examples from Terra and Aqua. *IEEE Transactions on Geoscience and Remote Sensing*, 55(1), 502–525. https://doi.org/10.1109/tgrs.2016.2610522
- Reid, E. A., Reid, J. S., Meier, M. M., Dunlap, M. R., Cliff, S. S., Broumas, A., et al. (2003). Characterization of African dust transported to Puerto Rico by individual particle and size segregated bulk analysis. *Journal of Geophysical Research*, 108, 8591. https://doi.org/10.1029/ 2002JD002935
- Ryder, C. L., Highwood, E. J., Rosenberg, P. D., Trembath, J., Brooke, J. K., Bart, M., et al. (2013). Optical properties of Saharan dust aerosol and contribution from the coarse mode as measured during the Fennec 2011 aircraft campaign. Atmospheric Chemistry and Physics, 13(1), 303–325. https://doi.org/10.5194/acp-13-303-2013
- Ryder, C. L., Highwood, E. J., Walser, A., Seibert, P., Philipp, A., & Weinzierl, B. (2019). Coarse and giant particles are ubiquitous in Saharan dust export regions and are radiatively significant over the Sahara. Atmospheric Chemistry and Physics, 19(24), 15353–15376. https://doi.org/10.5194/acp-19-15353-2019
- Ryder, C. L., Marenco, F., Brooke, J. K., Estelles, V., Cotton, R., Formenti, P., et al. (2018). Coarse-mode mineral dust size distributions, composition and optical properties from AER-D aircraft measurements over the tropical eastern Atlantic. Atmospheric Chemistry and Physics, 18(23), 17225–17257. https://doi.org/10.5194/acp-18-17225-2018
- Ryder, C. L., McQuaid, J. B., Flamant, C., Rosenberg, P. D., Washington, R., Brindley, H. E., et al. (2015). Advances in understanding mineral dust and boundary layer processes over the Sahara from Fennec aircraft observations. Atmospheric Chemistry and Physics, 15(14), 8479–8520. https://doi.org/10.5194/acp-15-8479-2015
- Saito, M., Yang, P., Ding, J., & Liu, X. (2021). A comprehensive database of the optical properties of irregular aerosol particles for radiative transfer simulations. *Journal of the Atmospheric Sciences*, 78, 2089–2111. https://doi.org/10.1175/jas-d-20-0338.1
- Schuster, G. L., Vaughan, M., MacDonnell, D., Su, W., Winker, D., Dubovik, O., et al. (2012). Comparison of CALIPSO aerosol optical depth retrievals to AERONET measurements, and a climatology for the lidar ratio of dust. *Atmospheric Chemistry and Physics*, 12(16), 7431–7452. https://doi.org/10.5194/acp-12-7431-2012
- Sinyuk, A., Holben, B. N., Eck, T. F., Giles, D. M., Slutsker, I., Korkin, S., et al. (2020). The AERONET Version 3 aerosol retrieval algorithm, associated uncertainties and comparisons to Version 2. Atmospheric Measurement Techniques, 13(6), 3375–3411. https://doi.org/10.5194/amt-13-3375-2020
- Smith, N., & Barnet, C. D. (2023). Practical implications of CLIMCAPS cloud clearing and derived quality metrics. *Earth and Space Science*, 10(6), e2023EA002913. https://doi.org/10.1029/2023ea002913
- Song, Q., Zhang, Z., Yu, H., Kato, S., Yang, P., Colarco, P., et al. (2018). Net radiative effects of dust in the tropical North Atlantic based on integrated satellite observations and in situ measurements. *Atmospheric Chemistry and Physics*, 18(15), 11303–11322. https://doi.org/10.5194/
- Stamnes, K., Tsay, S. C., Wiscombe, W., & Jayaweera, K. (1988). Numerically stable algorithm for discrete-ordinate-method radiative transfer in multiple scattering and emitting layered media. *Applied Optics*, 27(12), 2502–2509. https://doi.org/10.1364/ao.27.002502
- Stein, A., Draxler, R. R., Rolph, G. D., Stunder, B. J., Cohen, M., & Ngan, F. (2015). NOAA's HYSPLIT atmospheric transport and dispersion modeling system. *Bulletin of the American Meteorological Society*, 96(12), 2059–2077. https://doi.org/10.1175/bams-d-14-00110.1
- Tegen, I., & Fung, I. (1994). Modeling of mineral dust in the atmosphere: Sources, transport, and optical thickness. *Journal of Geophysical Research*, 99(D11), 22897–22914. https://doi.org/10.1029/94jd01928
- Toledano, C., Torres, B., Velasco-Merino, C., Althausen, D., Groß, S., Wiegner, M., et al. (2019). Sun photometer retrievals of Saharan dust properties over Barbados during SALTRACE. Atmospheric Chemistry and Physics, 19(23), 14571–14583. https://doi.org/10.5194/acp-19-14571-2019
- Torres, B., Dubovik, O., Fuertes, D., Schuster, G., Cachorro, V. E., Lapyonok, T., et al. (2017). Advanced characterisation of aerosol size properties from measurements of spectral optical depth using the GRASP algorithm. *Atmospheric Measurement Techniques*, 10, 3743–3781. https://doi.org/10.5194/amt-10-3743-2017
- Torres, B., & Fuertes, D. (2021). Characterization of aerosol size properties from measurements of spectral optical depth: A global validation of the GRASP-AOD code using long-term AERONET data. Atmospheric Measurement Techniques, 14(6), 4471–4506. https://doi.org/10.5194/ amt-14-4471-2021
- Turner, D. D. (2005). Arctic mixed-phase cloud properties from AERI lidar observations: Algorithm and results from SHEBA. *Journal of Applied Meteorology*, 44(4), 427–444. https://doi.org/10.1175/jam2208.1
- van der Does, M., Korte, L. F., Munday, C. I., Brummer, G. J. A., & Stuut, J. B. W. (2016). Particle size traces modern Saharan dust transport and deposition across the equatorial North Atlantic. *Atmospheric Chemistry and Physics*, 16(21), 13697–13710. https://doi.org/10.5194/acp-16-13697-2016
- Wang, C., Yang, P., Platnick, S., Heidinger, A. K., Baum, B. A., Greenwald, T., et al. (2013). Retrieval of ice cloud properties from AIRS and MODIS observations based on a fast high-spectral-resolution radiative transfer model. *Journal of Applied Meteorology and Climatology*, 52(3), 710–726. https://doi.org/10.1175/jamc-d-12-020.1

ZHENG ET AL. 11 of 12

- Weinzierl, B., Ansmann, A., Prospero, J. M., Althausen, D., Benker, N., Chouza, F., et al. (2017). The Saharan aerosol long-range transport and aerosol–cloud-interaction experiment: Overview and selected highlights. *Bulletin of the American Meteorological Society*, 98(7), 1427–1451. https://doi.org/10.1175/bams-d-15-00142.1
- Weinzierl, B., Sauer, D., Esselborn, M., Petzold, A., Veira, A., Rose, M., et al. (2011). Microphysical and optical properties of dust and tropical biomass burning aerosol layers in the Cape Verde region—An overview of the airborne in situ and lidar measurements during SAMUM-2. *Tellus B: Chemical and Physical Meteorology*, 63(4). https://doi.org/10.3402/tellusb.v63i4.16350
- Welton, E., Campbell, J., Spinhirne, J., & Scott, V. S. (2001). Global monitoring of clouds and aerosols using a network of micropulse lidar systems. SPIE.
- Welton, E. J., Stewart, S. A., Lewis, J. R., Belcher, L. R., Campbell, J. R., & Lolli, S. (2018). Status of the NASA Micro pulse lidar network (MPLNET): Overview of the network and future plans, new version 3 data products, and the polarized MPL. EPJ Web of Conferences, 176, 09003. https://doi.org/10.1051/epjconf/201817609003
- Welton, E. J., Voss, K. J., Gordon, H. R., Maring, H., Smirnov, A., Holben, B., et al. (2000). Ground-based lidar measurements of aerosols during ACE-2: Instrument description, results, and comparisons with other ground-based and airborne measurements. *Tellus B: Chemical and Physical Meteorology*, 52(2), 636–651. https://doi.org/10.1034/j.1600-0889.2000.00025.x
- Yang, P., Feng, Q., Hong, G., Kattawar, G. W., Wiscombe, W. J., Mishchenko, M. I., et al. (2007). Modeling of the scattering and radiative properties of nonspherical dust-like aerosols. *Journal of Aerosol Science*, 38(10), 995–1014. https://doi.org/10.1016/j.jaerosci.2007.07.001
- Yu, H., Chin, M., Bian, H., Yuan, T., Prospero, J. M., Omar, A. H., et al. (2015). Quantification of trans-Atlantic dust transport from seven-year (2007–2013) record of CALIPSO lidar measurements. *Remote Sensing of Environment*, 159, 232–249. https://doi.org/10.1016/j.rse.2014.
- Zheng, J., Zhang, Z., Garnier, A., Yu, H., Song, Q., Wang, C., et al. (2022). The thermal infrared optical depth of mineral dust retrieved from integrated CALIOP and IIR observations. Remote Sensing of Environment, 270, 112841. https://doi.org/10.1016/j.rse.2021.112841
- Zheng, J., Zhang, Z., Yu, H., Garnier, A., Song, Q., Wang, C., et al. (2023). Thermal infrared dust optical depth and coarse-mode effective diameter over oceans retrieved from collocated MODIS and CALIOP observations. Atmospheric Chemistry and Physics, 23(14), 8271–8304. https://doi.org/10.5194/acp-23-8271-2023
- Zhou, Y., Levy, R. C., Remer, L. A., Mattoo, S., & Espinosa, W. R. (2020). Dust aerosol retrieval over the oceans with the MODIS/VIIRS dark target algorithm: 2. Nonspherical dust model. *Earth and Space Science*, 7(10), e2020EA001222. https://doi.org/10.1029/2020ea001222

ZHENG ET AL. 12 of 12